Catalytic CO oxidation on nanoscale Pt facets: Effect of interfacet CO diffusion on bifurcation and fluctuation behavior

N. Pavlenko,[1,*] J. W. Evans,[2,3] Da-Jiang Liu,[2] and R. Imbihl[1]
[1]*Institut für Physikalische Chemie und Elektrochemie, Universität Hannover, Callinstrasse 3-3a, D-30167 Hannover, Germany*
[2]*Ames Laboratory, Iowa State University, Ames, Iowa 50011*
[3]*Department of Mathematics, Iowa State University, Ames, Iowa 50011*
(Received 28 June 2001; published 18 December 2001)

We present lattice-gas modeling of the steady-state behavior in CO oxidation on the facets of nanoscale metal clusters, with coupling via interfacet CO diffusion. The model incorporates the key aspects of the reaction process, such as rapid CO mobility within each facet and strong nearest-neighbor repulsion between adsorbed O. The former justifies our use of a ''hybrid'' simulation approach treating the CO coverage as a mean-field parameter. For an isolated facet, there is one bistable region where the system can exist in either a reactive state (with high oxygen coverage) or a (nearly CO-poisoned) inactive state. Diffusion between two facets is shown to induce complex multistability in the steady states of the system. The bifurcation diagram exhibits two regions with bistabilities due to the difference between adsorption properties of the facets. We explore the role of enhanced fluctuations in the proximity of a cusp bifurcation point associated with one facet in producing transitions between stable states on that facet, as well as their influence on fluctuations on the other facet. The results are expected to shed more light on the reaction kinetics for supported catalysts.

DOI: 10.1103/PhysRevE.65.016121 PACS number(s): 05.10.−a, 05.45.−a, 82.65.+r, 05.40.−a

I. INTRODUCTION

A central problem in the modeling of catalytic surface reactions is to bridge the gap between the studies of reactions on ideal homogeneous surfaces of macroscopic sizes and real catalytic processes on supported catalysts. The latter are composed of small nm-sized metallic clusters on an inert support material. The surface of these clusters contains facets of different orientations, and hence differing reactivities, which are coupled, e.g., through diffusion of mobile adsorbates. Due to this coupling effect, and since fluctuations in such small-sized facets can become dominant, the behavior of these systems can differ strongly from that predicted by mean-field rate laws on ideal single-crystal surface planes. An understanding of the effects that can arise is crucial not only for the modeling of real catalysis, but also for the design of nanostructured catalysts.

For catalytic CO oxidation, by far the majority of experimental studies have been performed on extended single-crystal substrates. Mean-field equations, ignoring spatial correlations and ordering in surface adlayers, have been successfully applied to predict a wide variety of surface phenomena, including nonlinear dynamics and spatial pattern formation [1]. More sophisticated lattice-gas models can be utilized to describe the effect of adspecies interactions, and ''hybrid'' formulations can treat directly and efficiently rapid surface diffusion of some adsorbates such as CO (the rate of CO diffusion is of many orders of magnitude higher than the rates of adsorption, desorption, and O diffusion). A recently developed canonical hybrid lattice-gas model of this type for CO oxidation incorporates a random distribution of CO and strong nearest-neighbor O repulsion [2–4].

In situ experimental studies of reactions on supported catalysts are still beyond the imaging capabilities of current microscopes. However, for a reasonable model system, as far as the dimension of the facets and the coupling of different orientations are concerned, one can consider reactions on a field emitter tip. The surface of such a tip can be imaged with field electron/field ion microscopy with nearly nanometer/atomic resolution. In a series of recent experiments, the spatiotemporal dynamics of the fluctuations which arise in catalytic CO oxidation on a Pt tip have been studied in some detail [5].

Conventional or hybrid lattice-gas modeling is ideally suited to analyze both kinetics and fluctuations in nanoscale systems [5,6]. For example, recent modeling of reaction kinetics on the facets coupled by reactant diffusion reveals shifts in the reaction window for bistable systems, and shifts in the oscillation window for systems that incorporate additional feedback. The latter also indicates a possible transition from regular to chaotic oscillations due to additional reactants from the adjacent facet [6]. Lattice-gas modeling has also been applied to analyze fluctuations in catalytic CO oxidation within a small isolated facet containing hundreds to thousands of adsorption sites [5]. What has been neglected in these studies [5] is the coupling between adjacent facets on the Pt field-emitter tip. Experimentally, there is some justification for this, since one observes that fluctuations on different facets were usually largely uncorrelated (while a high degree of spatial correlations exists only for fluctuations on a single facet). One can in fact explain this behavior noting that CO diffusion is very fast within a facet, but inhibited by structural heterogeneities (such as atomic steps) at the periphery of the facet. However, there is some coupling between facets, as the kinetics is described by a global bifur-

*Present address: Institut für Theoretische Physik T34, Physik-Department der TU München, James-Franck St., D-85747 Garching, Germany.

cation diagram, and there must be some correlation between the fluctuations.

Thus, to shed more light on reaction behavior for coupled nanoscale facets, we focus in this work on incorporation of interfacet diffusion into the above-mentioned canonical model describing key aspects of CO oxidation. We find that the diffusive coupling between two adjacent facets with different adsorption properties results in the appearance of complex multistability of the steady states (which is fully characterized exploiting a novel simulation approach). Consequently, the bifurcation diagram exhibits two regions with bistabilities instead of the single bistable region observed in the case of an isolated facet. We show that typically the different facets have different fluctuation characteristics. However, in some cases, the diffusion-induced coupling can change radically the fluctuation behavior of the whole system, producing a transition between stable states on one facet induced by enhanced fluctuations on the other facet.

II. THE TWO-FACET REACTION MODEL AND ITS ANALYSIS

A. Model specification

The lattice-gas model employed for our studies is based on the Langmuir-Hinshelwood mechanism for catalytic CO oxidation. The two ''adjacent'' small facets labeled $i=1,2$ are represented by two rectangular grids of $N_i=L_0\times L_i$ adsorption sites. One could physically connect the facets, e.g., at a common edge of length L_0, which would introduce spatial inhomogeneity within each facet. However, we adopt a simplified treatment invoking periodic boundary conditions. We incorporate the following steps into a ''hybrid'' model [2,3], adapted here for the two-facet case.

(i) CO(gas) adsorbs onto single empty sites at a rate p_{CO} per site on both facets, and desorbs at a rate d. CO(ads) can hop very rapidly to other empty sites within each facet. Since we consider below the regime of infinitely mobile CO(ads) within the facets, and neglect interactions between CO(ads) and other CO(ads) and O(ads), the distribution of CO(ads) on sites not occupied by O(ads) is random. Thus, in our simulation procedure, we track only the total numbers N_{CO}^1 and N_{CO}^2 of CO(ads) on each facet, whereas the distribution of O(ads) for each facet is described by a full lattice-gas approach.

(ii) CO(ads) can diffuse at a finite rate from each facet to empty sites on the adjacent facet. Physically, CO(ads) would hop across a common edge (of length L_0) to adjacent empty sites at rate, say, h'. In our model with periodic boundary conditions, this mass transport is mimicked by transport of CO(ads) from facet i to j at rate (in molecules per unit time) $h^i N_{\mathrm{CO}}^i$ times the probability that a site is empty on facet j, where $h^i=h'/L_i$.

(iii) O_2(gas) adsorbs dissociatively at the impingement rate p_{O_2} per site (as described below), but the sticking coefficients for oxygen differ for each facet: $s_{\mathrm{O}}^1\neq s_{\mathrm{O}}^2$ so that the two facets exhibit a different catalytic activity. To account for very strong NN O(ads)-O(ads) repulsions, we invoke an ''eight-site rule'' [7] wherein O_2(gas) adsorbs only at diagonal nearest-neighbor (NN) empty sites, provided that the additional six sites adjacent to these are not occupied by O(ads). Also, O(ads) is immobile, and cannot desorb, and thus never occupies adjacent sites within each facet.

(iv) Adjacent pairs of CO(ads) and O(ads) within a facet react at rate k to form CO_2(gas), which desorbs immediately.

As in the single-facet case, we set $p_{\mathrm{CO}}+p_{\mathrm{O}_2}=k=1$ and consider system behavior as a function of p_{CO} with $p_{\mathrm{O}_2}=1-p_{\mathrm{CO}}$. In contrast to the simplified ZGB (Ziff-Gulari-Barshad) model [8], where CO(ads) is immobile, the main feature of the above model when applied to a single isolated facet is the appearance of strong bistability: over a significant range of p_{CO} and (smaller) d values, there is both a stable reactive state (with high O coverage Θ_{O}) and a stable inactive state (with the surface nearly poisoned by CO).

B. Constant-partial-pressure (standard) and constant-coverage (refined) simulations

Standard ''constant (partial) pressure'' kinetic Monte Carlo (KMC) simulations simply implement all processes (adsorption, desorption, reaction, and diffusion) with the appropriate relative rates. They can be readily implemented for single and coupled facet models, and enable analysis of stable steady states as well as kinetics. To also analyze the nontrivial UNSTABLE steady states existing in bistable (or multistable) regions, a constant-coverage algorithm [9] has been applied previously for large single-facet systems. In the adsorption part of the algorithm, instead of attempting to deposit with the appropriate relative rates, these simulations specify a target CO coverage Θ_{CO}, and deposit CO (O) for actual CO coverages below (above) this target. Then the asymptotic p_{CO} value (corresponding to given Θ_{CO}) is found as a fraction of attempts to deposit CO. In our case of two communicating facets with different O sticking properties, the above constant-coverage approach is unsuitable: fixing the CO coverage on both facets corresponds to different values of p_{CO} (which is unphysical). To resolve this problem, in this work we develop a combined constant-pressure and constant-coverage algorithm. Analysis using this novel simulation procedure is performed in two steps.

First, we fix a target CO coverage for the first facet Θ_{CO}^1, but use the constant-pressure algorithm for the second facet (where the pressure is determined by the impingement rates for the first facet). Fixing Θ_{CO}^1 during this step allows us to probe both stable states together with the unstable state in the bistability region on the first facet, but the CO coverage on the second facet Θ_{CO}^2 relaxes with time to a stable steady-state value corresponding to the rate p_{CO} (which is equal for both facets). Because of this feature, we cannot probe the unstable state on the second facet in the bistable region (the same limitation as in constant-pressure simulations).

Second, to probe the full set of states on the second facet (including the unstable state), we invert the above procedure, prescribing the coverage Θ_{CO}^2 and performing standard constant-pressure simulations on the first facet. This gives us all states for the second facet, but just the stable states for the first one (matching results from above). Thus, whereas the first step gives us the full picture for the first facet and in-

complete data for the second one, after performing both steps, we can obtain the full picture (i.e., the complete bifurcation diagram) for the whole system.

C. Analytic pair-approximation treatment

Our novel simulation procedure extends conventional KMC approaches in order to obtain complete steady-state behavior. It is thus natural to compare results with those obtained from analysis of (approximate) rate equations for our two-facet CO oxidation (which automatically provides complete steady-state information). For convenience, we denote adsorbed CO by A and adsorbed O by B, using standard notation for the monomer-dimer $A+B_2$ reaction model. Following [3], we let E denote empty sites, $Z=1-B$ denote sites not occupied by B, and indicate probabilities of various configurations by square brackets. Then, for CO and O coverages on the ith facet ($i=1,2$) of $\Theta^i_{\rm CO}=[A_i]$ and $\Theta^i_{\rm O}=[B_i]$, respectively, the rate equations have the following form:

$$\frac{d}{dt}[A_i]=p_{\rm CO}[E_i]-d[A_i]-4k[A_iB_i]-h^iJ_i, \tag{1}$$

$$\frac{d}{dt}[B_i]=2p_{\rm O_2}s^i_{\rm O}\begin{bmatrix} & & Z & \\ & Z & E & Z \\ Z & E & Z & \\ & Z & & \end{bmatrix}-4k[A_iB_i] \quad (i=1,2).$$

The net diffusive CO flux $J_1=-J_2=[A_1E_2]-[A_2E_1]=[A_1(1-B_2)]-[A_2(1-B_1)]$ introduced in Eqs. (1) describes the CO transport between facets with the microscopic hop rate h' related to the h^i as described above. (In our analysis, we set $N_1=N_2$ corresponding to equal-sized facets, and thus $h^1=h^2=h$.) The lack of spatial correlations between facets further reduces J_i to $J_1=-J_2=[A_1](1-[B_2])-[A_2](1-[B_1])$. The lack of NN O(ads), together with the random distribution of CO within each facet, allows further reduction of Eqs. (1). For example, the reaction terms can be exactly expressed in terms of the coverages [3]:

$$[A_iB_i]=[A_i][B_i]/(1-[B_i]).$$

These results allow derivation of an exact relationship between $[A]$ and $[B]$ for the steady states ($d/dt[A_i]=0$) from the first equation in Eqs. (1):

$$[A_1]=-p_{\rm CO}(1-[B_1])\{h^1(1-[B_2])+b_1\}/c \quad \text{and}$$
$$[A_2]=-p_{\rm CO}(1-[B_2])\{h^2(1-[B_1])+b_2\}/c, \tag{2}$$

where $c=h^1h^2(1-[B_1])(1-[B_2])-b_1b_2$; $b_1=p_{\rm CO}+d+4k[B_2]/(1-[B_2])+h^2(1-[B_1])$; and $b_2=p_{\rm CO}+d+4k[B_1]/(1-[B_1])+h^1(1-[B_2])$. We next substitute the resulting expressions (2) for $[A_i]$ into the second equation in Eqs. (1) and apply the pair (Kirkwood-type) approximation [2,3] to decouple the eight-site correlation functions in Eqs. (1) describing the ''eight-site rule.'' The analysis of the steady states for two adjacent facets (corresponding to the conditions $d/dt[A_i]=0$ and $d/dt[B_i]=0$) is then reduced to solving the closed system of two high-order polynomial equations with respect to $[B_i]$, and subsequent evaluation of $[A_i]$ from Eqs. (2).

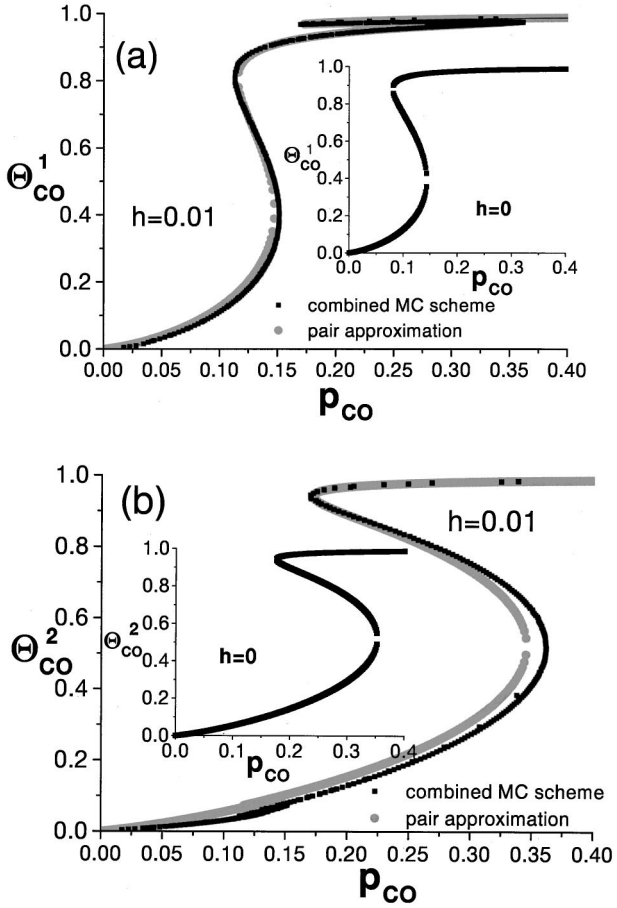

FIG. 1. $p_{\rm CO}$ dependences of CO converges for the facets coupled via CO diffusion with (a) $s^1_{\rm O}=0.2$ and (b) $s^2_{\rm O}=1.0$ at $d=0.005$ and $h=0.01$. The insets show the corresponding dependences for the isolated facets obtained with the pair approximation.

III. RESULTS FOR STEADY-STATE BIFURCATION BEHAVIOR

A. Case study: $s^1_{\rm O}=0.2$ and $s^2_{\rm O}=1.0$

We now present a brief overview of results from our KMC simulation procedure for coupled N_1+N_2 site facets, which are compared with pair-approximation predictions using rate equations (1). To demonstrate the effect of interfacet diffusion, for $h=0.01$, we show in Fig. 1 the CO coverages versus $p_{\rm CO}$ for $s^1_{\rm O}=0.2$ and $s^2_{\rm O}=1.0$. A very good agreement is found between results from KMC simulation and the pair approximation (1). The latter produces only slight deviation of bistable regions towards lower $p_{\rm CO}$. The difference between $[A_i]$ and $[B_i]$ obtained using both approaches is most significant in the reactive state, since the high O coverage makes the pair approximation for the ''eight-site rule'' less accurate. In contrast to the case of isolated facets when h

$=0$ (shown in the insets of Fig. 1), a qualitatively new feature appears in Θ_{CO}^{1} and Θ_{CO}^{2} behavior due to the interfacet communication by CO hopping. Besides the bistability region (no. 1) for $0.113 \leqslant p_{CO} \leqslant 0.1515$ on the first facet with $s_O^1 = 0.2$ (resembling closely that for $h=0$), an additional bistable region (no. 2) at $0.17 \leqslant p_{CO} \leqslant 0.3614$ forms on the first facet covered predominantly by CO. This is a response to the bistable behavior in this range of p_{CO} values occurring on the second facet with $s_O^2 = 1.0$. Analogously, an additional bistable region on the second facet for $0.113 \leqslant p_{CO} \leqslant 0.1515$ arises in the state with low CO coverage as a response to a bistable behavior on the first facet.

Figure 2 shows the variation with h of the bifurcation diagrams in the (p_{CO},d) plane. For low diffusion rate h, the phase diagram contains two overlapping bistable regions [see Fig. 2(a)]: the small region No. 1 at lower p_{CO} terminating at the cusp point $(p_c^1 \approx 0.1548, d_c^1 \approx 0.025)$ originates from the first facet $(s_O^1 = 0.2)$, whereas the larger region No. 2 terminating at the cusp point $(p_c^2 \approx 0.409, d_c^2 \approx 0.051)$ occurs due to the second facet. Note that the behavior of both bistable regions differs dramatically with varying h. The larger region No. 2 varies only weakly with h, whereas the smaller region No. 1 first shrinks and then disappears. The latter behavior can be understood as CO on the first facet is supplied very rapidly to the second facet with lower CO coverage, thus suppressing completely the occurrence of region No. 1.

B. Dependence of behavior on sticking probabilities

In extending our analysis to general s_O values, we introduce three different coupling regimes: (i) $0<h<h_1$, weak-coupling regime when two overlapping bistable regions cross each other on the diagram (p_{CO},d); (ii) $h_1<h<h_2$, medium-coupling regime with one smaller bistability located completely inside another larger one; (iii) $h>h_2$, strong-coupling regime with only one common bistable region. This classification will be valuable for the studies of fluctuation behavior below. The values h_1 and h_2 separating these regimes are shown in Fig. 3(a) as a function of s_O^1 (at $s_O^2 = 1.0$). As $s_O^1 \to 0$, obviously both h_1 and h_2 go to 0 (since the first facet becomes an oxygen-free "sink" for CO, and thus the bistability region No. 1 disappears). See the inset of Fig. 3(a).

The variation of h_1 and h_2 with s_O^1 shows three distinct branches arising from competition between the effects of (i) the inequality in oxygen sticking and (ii) finite interfacet transport. The *first branch* $(s_O^1 < 0.65)$ is formed due to the increased s_O^1 value providing the expansion of the first smaller bistable region No. 1. As the difference in oxygen sticking properties $|s_O^1 - s_O^2|$ decreases, the *second branch* $(0.65 < s_O^1 < 1)$ appears due to a dominant role of restricted interfacet transport. We comment in particular on the case $s_O^1 = s_O^2 = 1$ (identical facets) where $h_2 \approx 0.06 \neq 0$, and where one might expect just one bistable region (so $h_2 = 0$). Indeed, the "symmetric" steady states for a single facet must apply to this system, but restricted interfacet transport produces two additional "unsymmetric" stable steady states [see Fig. 3(b), inset]. The region of the existence of these two states

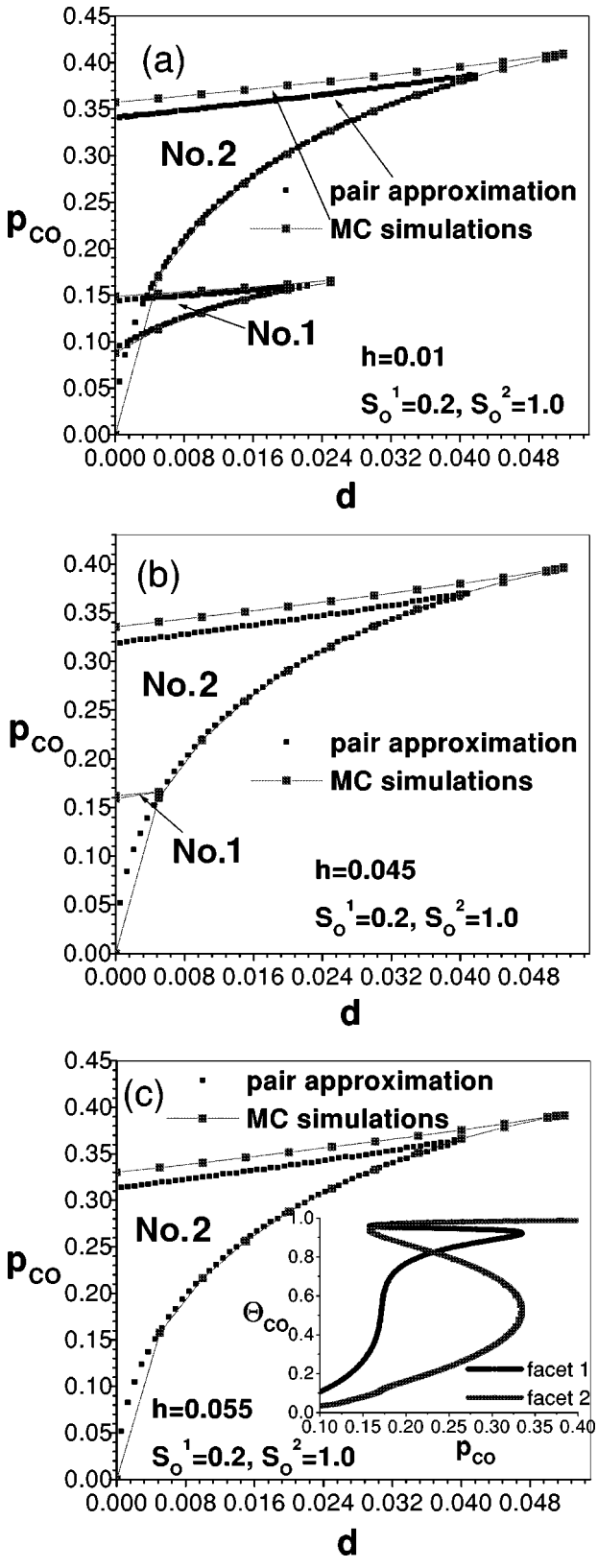

FIG. 2. Bifurcation diagrams (p_{CO},d) showing the bistable regions No. 1 and No. 2, calculated for different coupling regimes at $s_O^1 = 0.2$ and $s_O^2 = 1.0$.

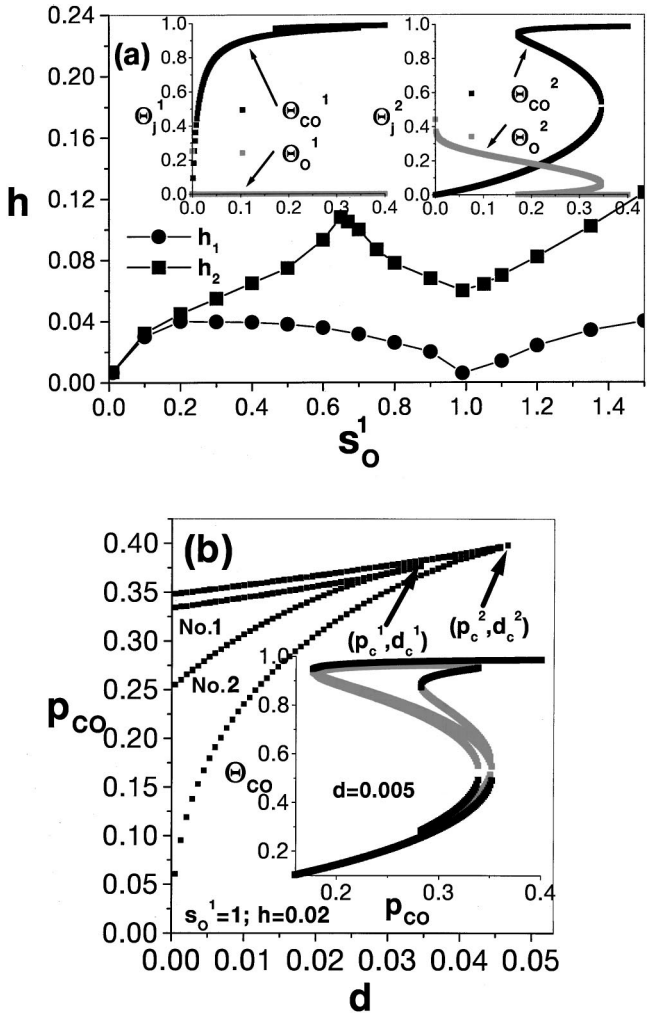

FIG. 3. Dependence of the critical parameters h_1 and h_2 on the s_O^1 at fixed $s_O^2=1.0$. The insets show p_{CO} dependences of the steady-state CO coverages on the two facets at $s_O^1=0$, $s_O^2=1.0$, and $h=0.02$. (b) Bifurcation diagram calculated using the pair approximation at $s_O^1=s_O^2=1$ and $h=0.01$ (medium-coupling regime). No. 1 and No. 2 indicate bistable region No. 1 (where both "unsymmetric" steady states are stable) and bistable region No. 2, respectively. The inset shows the corresponding p_{CO} dependence of $\Theta_{CO}^1=\Theta_{CO}^2=\Theta_{CO}$ obtained at $d=0.005$ with the stable and unstable states indicated by black and gray, respectively.

located inside the large bistable region no. 2 is indicated on the bifurcation diagram in Fig. 3(b). For the *third branch* ($s_O^1>1$), the inequality in sticking again begins to be of primary importance producing the increase in h_1 and h_2 shown in Fig. 3(a).

IV. RESULTS FOR FLUCTUATION BEHAVIOR

Bearing in mind the classification of coupling regimes in Sec. III B, we turn now to an analysis of the coverage fluctuations. The fluctuation amplitudes depend inversely on system size, and become more significant approaching a cusp critical point (analogous to fluctuation behavior near a critical point in equilibrium thermodynamics). Thus, they can induce transitions between the stable steady states for systems that are small enough or in close proximity to a cusp point [5,10]. Here, we consider two coupled facets, each with 30×30 lattice sites, and analyze fluctuation effects both for different coupling regimes and for different s_O^1 values at fixed $s_O^2=1.0$. As already noted, the size and location of the small bistability region No. 1 depends strongly on the value of $|s_O^1-s_O^2|$. We show below that this factor, together with the coupling strength (h), strongly influences fluctuation behavior. We consider separately two regimes of coupling strength.

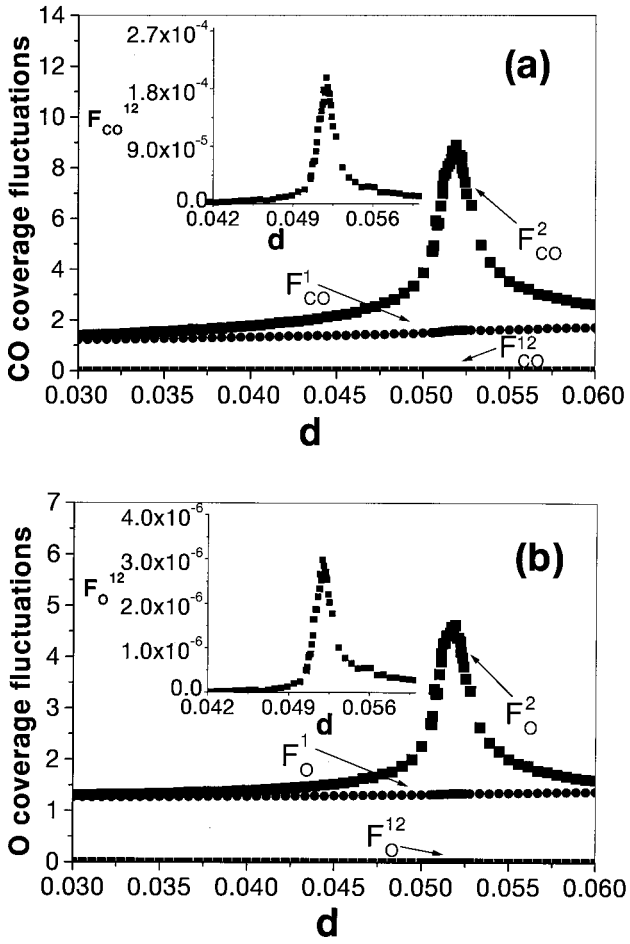

FIG. 4. Normalized amplitudes $F_j^i=\{N_i\langle(\delta\Theta_j^i)^2\rangle/[\langle\Theta_j^i\rangle(1-\langle\Theta_j^i\rangle)]\}^{1/2}$ and correlations $F_j^{12}=\langle\Theta_j^1\Theta_j^2\rangle-\langle\Theta_j^1\rangle\langle\Theta_j^2\rangle$ of coverage fluctuations on weakly coupled facets for species $j=$CO and O vs d for $p_{CO}\approx0.4096$ close to the cusp point of bistability No. 1 ($h=0.005$, $s_O^1=0.7$, $s_O^2=1.0$); $L=60$ and 700 000 MC steps are taken for combined MC procedure.

A. Weak-coupling regime

In Fig. 4, we plot the normalized amplitudes

$$F_j^i=\{N_i\langle(\delta\Theta_j^i)^2\rangle/[\langle\Theta_j^i\rangle(1-\langle\Theta_j^i\rangle)]\}^{1/2}\quad(j=\mathrm{CO},\ \mathrm{O})$$

($\langle\Theta_j^i\rangle$ denote the time averages of $\Theta_j^i=N_j^i/N_i$ and $\delta\Theta_j^i=\Theta_j^i-\langle\Theta_j^i\rangle$) versus d on both facets close to the cusp point (p_c^2,d_c^2) terminating the large bistability region No. 2 for $s_O^1=0.7$ and $h=0.005$ (in this case $p_c^2\approx0.4096$). As d approaches d_c^2, the amplitudes F_j^2 increase drastically, whereas

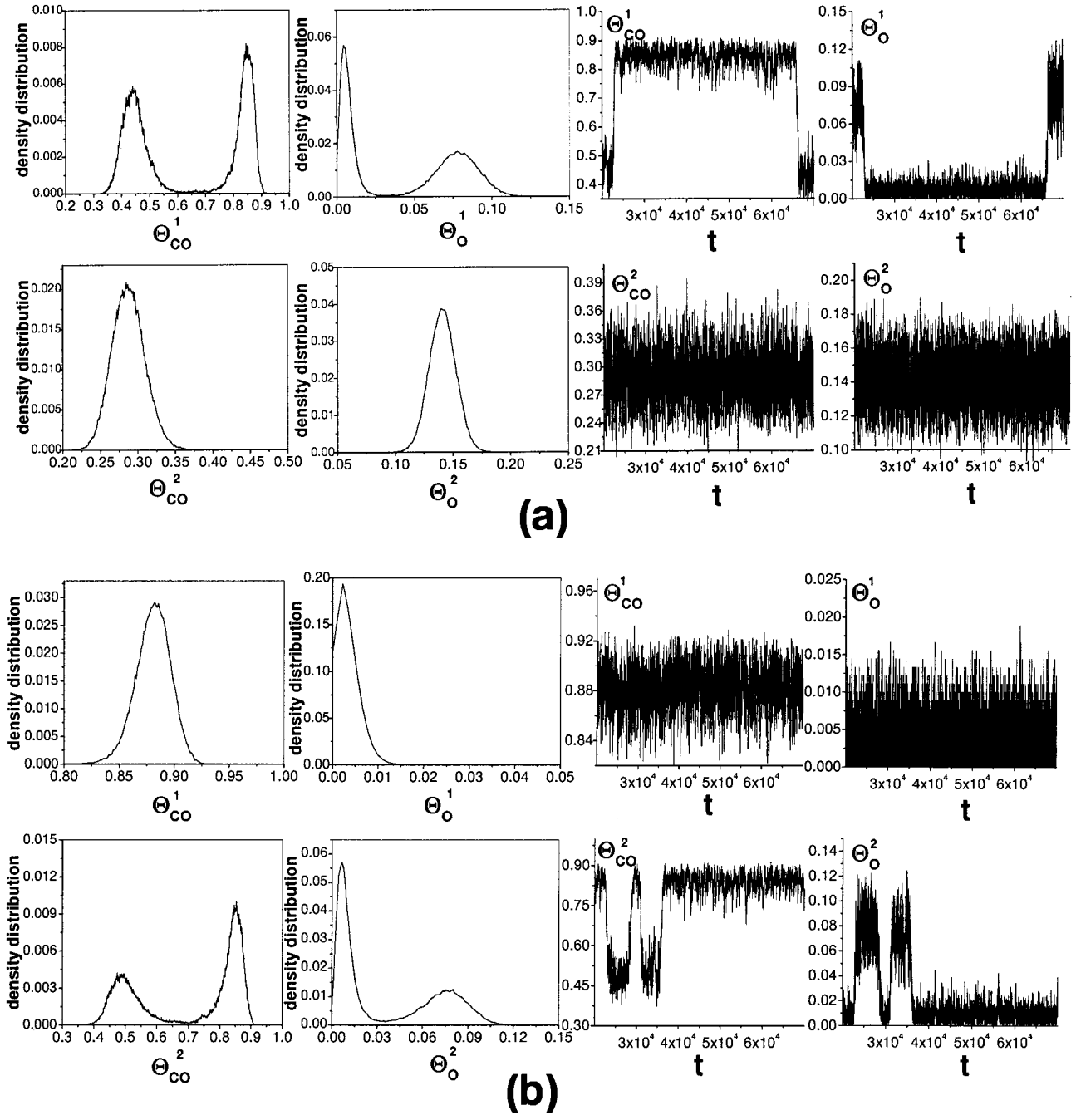

FIG. 5. Time series and distributions of Θ_j^i close to midpoint of (a) bistable region No. 1, (b) bistable region No. 2 ($h=0.005$, $s_O^1=0.7$, $s_O^2=1.0$).

just a slight increase of F_j^1 is observed with $d \to d_c^2$, reflecting a very weak response of the first facet on the critical behavior of the second facet. Moreover, we find that correlations between fluctuations on the different facets (measured by $F_j^{12}=\langle\Theta_j^1\Theta_j^2\rangle-\langle\Theta_j^1\rangle\langle\Theta_j^2\rangle$; see Fig. 4, insets) are practically zero compared to correlations within each facet (measured by F_j^i). An analogous (but reversed) picture emerges close to the other cusp point. This behavior is consistent with the observed weak correlation between fluctuations on different facets of Pt field-emitter tips [5].

The distinct character of fluctuations on different facets is also clear when analyzing time series for Θ_j^1 and Θ_j^2, or the normalized probability distributions $P(\Theta_j^i)$ [with $\int dx\, P(x)=1$]. Figure 5 shows $P(\Theta_j^i)$ obtained near the midpoints of the first and second bistable regions close to cusp points. For a fixed simulation time, as d approaches d_c^1 from below, the distributions of Θ_{CO}^1 and Θ_O^1 become bimodal [Fig. 5(a)], reflecting a transition between reactive and inactive states on the first facet induced by increased fluctuations. However, the form of Θ_{CO}^2 and Θ_O^2 distributions remains effectively monomodal. Since the difference in Θ_j^2 in the two stable states of bistability region No. 1 on the second facet is very

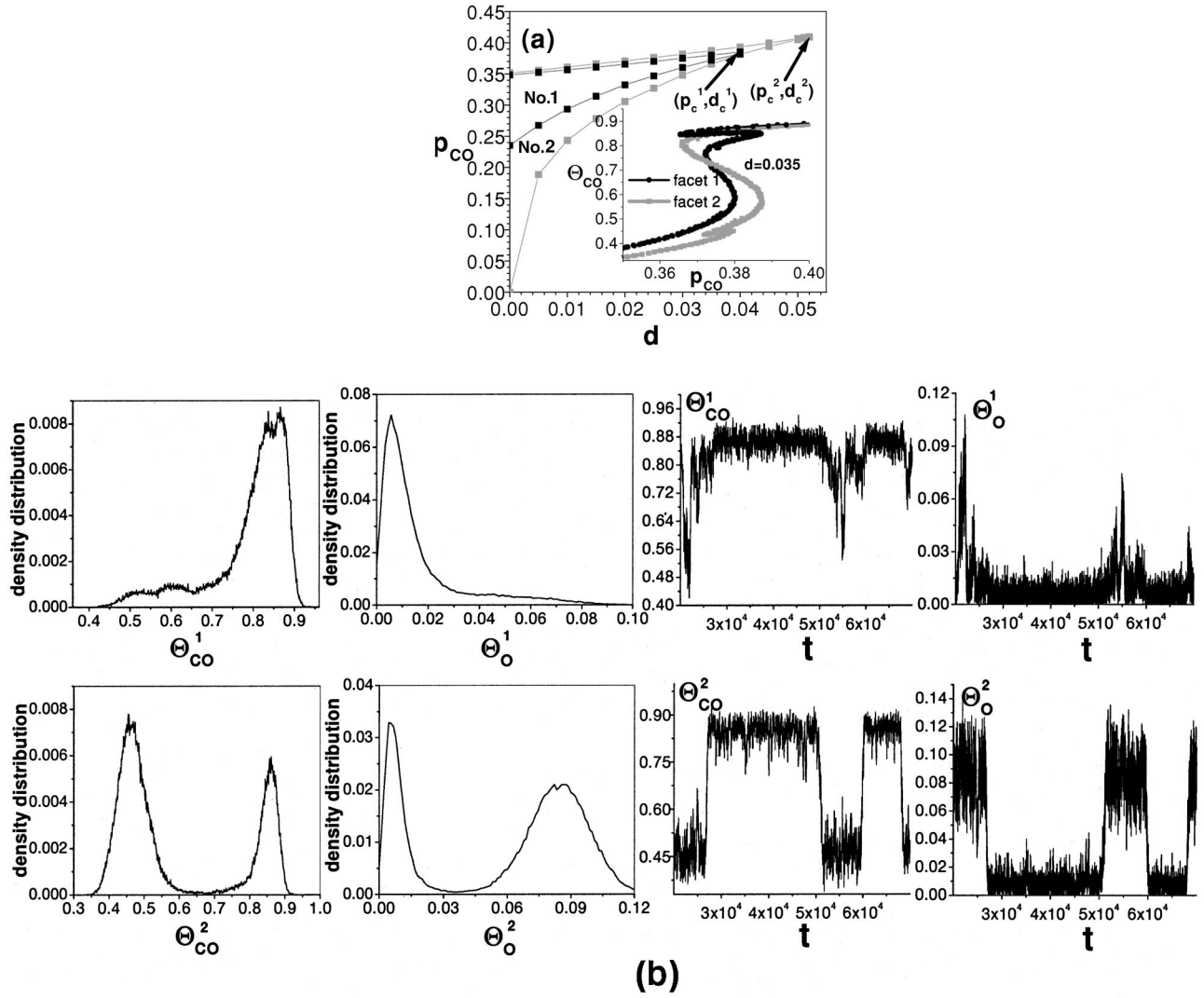

FIG. 6. (a) Bifurcation diagram calculated using combined MC scheme at $s_O^1=0.9$, $s_O^2=1.0$, and $h=0.018$ for the facets with medium coupling strength No. 1 and No. 2 indicate the bistability regions No. 1 and No. 2, respectively. The inset shows the stationary solutions Θ_{CO} vs p_{CO} on each facet at $d=0.035$. (b) Θ_j^i distributions and corresponding time series obtained at $d=0.035$ and $p_{CO}=0.375$ close to the cusp point of bistability No. 1 in the bifurcation diagram (a).

small (see coverages versus p_{CO} in Fig. 1), the transition between these states is practically invisible in the Θ_j^2 time series [Fig. 5(a)]. Analogous (but reversed) behavior is observed as $d \rightarrow d_c^2$ [Fig. 5(b)].

B. Medium-coupling regime

To study what happens when the cusp point (p_c^1, d_c^1) nears (p_c^2, d_c^2) in the (p_{CO}, d) plane, we consider next the medium-coupling regime when the difference $|s_O^1 - s_O^2|$ is small. We set $s_O^1=0.9$, $h=0.018$, and analyze the Θ_j^i time series close to the *first* cusp point $(p_c^1 \approx 0.383, d_c^1 \approx 0.04)$ of the bifurcation diagram shown in Fig. 6(a). Specifically, we examine the midpoint of the larger bistability region No. 2, close to the upper boundary of the inner region No. 1 [Fig. 6(b), $d=0.035$ and $p_{CO} \approx 0.375$]. Besides the conventional fluctuation-induced transition between two states with low and high Θ_{CO}^1 in bistability region No. 1 (for which Θ_{CO}^2 is always low, and thus distinct transitions in this quantity are masked), the time series for Θ_{CO}^1 show the occurrence of an additional transition between two states with high Θ_{CO}^1. These derive from bistability No. 2, as is clear from the corresponding transitions in the time series for Θ_j^2. This produces a rather complicated form of the distributions for Θ_{CO}^1, with additional peak splitting. Since the second cusp point (p_c^2, d_c^2) is close, corresponding fluctuations of the coverages in the states of region No. 2 on the first facet are sufficiently large to induce the additional transition. Note that the time series shown in Fig. 6(b) are synchronized for both facets due to the interfacet CO diffusion.

V. SUMMARY

We have shown that the diffusion of adsorbed CO between two small adjacent facets in catalytic CO oxidation leads to the appearance of complex multistability on each

facet. This replaces the conventional simpler bistability with coexisting reactive and inactive stable steady states. The additional stable steady states arise due to the difference in the sticking properties of the facets, and the finite rate of interfacet CO diffusion in our model (whereas the CO mobility within each facet is assumed to be infinite). The topology of bifurcation diagrams (p_{CO},d), as well as the effect of coverage fluctuations, are shown to be qualitatively different in regimes with different strengths of interfacet coupling. In the weak-coupling regime, the correlations between the fluctuations near the cusp points terminating bistable regions are low. However, in the medium-coupling regime, the transitions between the additional bistable states on each facet can occur due to the communication between facets via CO diffusion.

ACKNOWLEDGMENTS

N.P. gratefully acknowledges support of this research by the Alexander von Humboldt Foundation and thanks the Ames Laboratory for warm hospitality and providing computational facilities. D.J.L. and J.W.E. were supported for this work by the Division of Chemical Sciences, U.S. DOE, through Ames Laboratory (operated for the U.S. DOE by Iowa State University under Contract No. W-7405-Eng-82).

[1] R. Kapral and K. Showalter, *Chemical Waves and Patterns* (Kluwer, Dordrecht, 1995); R. Imbihl and G. Ertl, Chem. Rev. **95**, 697 (1995).
[2] M. Tamarro, M. Sabella, and J. W. Evans, J. Chem. Phys. **103**, 10 277 (1995).
[3] E. W. James, C. Song, and J. W. Evans, J. Chem. Phys. **111**, 6579 (1999).
[4] V. P. Zhdanov and B. Kasemo, Surf. Sci. **412/413**, 527 (1998).
[5] Yu. Suchorski, J. Beben, E. W. James, J. W. Evans, and R. Imbihl, Phys. Rev. Lett. **82**, 1907 (1999); Yu. Suchorski, J. Beben, R. Imbihl, E. W. James, Da-Jiang Liu, and J. W. Evans, Phys. Rev. B **63**, 165417 (2001).
[6] V. P. Zhdanov and B. Kasemo, Surf. Sci. Rep. **39**, 25 (2000).
[7] C. R. Brundle, R. J. Behm, and J. A. Barker, J. Vac. Sci. Technol. A **2**, 1038 (1984); S.-L. Chang and P. A. Thiel, Phys. Rev. Lett. **59**, 296 (1987).
[8] R. M. Ziff, E. Gulari, and Y. Barshad, Phys. Rev. Lett. **56**, 2553 (1986).
[9] R. M. Ziff and B. J. Brosilow, Phys. Rev. A **46**, 4630 (1992).
[10] K. Fichthorn, E. Gulari, and R. Ziff, Phys. Rev. Lett. **63**, 1527 (1989).